Heliyon 10 (2024) e30500

Contents lists available at ScienceDirect

Heliyon

journal homepage: www.cell.com/heliyon

Research article

Synergistic effect of Silver-Nanodiamond composite as an efficient antibacterial agent against *E. coli* and *S. aureus*

Saman Iqbal [a,*], Muhammad Shahid Rafique [b], Nida Iqbal [c], Sultan Akhtar [d], Aftab Ahmad Anjum [e], M.B. Malarvili [f,**]

[a] *Department of Physics, University of the Punjab, Lahore, Pakistan*
[b] *Department of Physics, University of Engineering and Technology, Lahore, Pakistan*
[c] *Biomedical Engineering Centre, University of Engineering and Technology, Lahore, Kala Shah Kaku (KSK) Campus, Pakistan*
[d] *Department of Biophysics, Institute for Research and Medical Consultations, Imam Abdulrahman bin Faisal University, Dammam, Saudi Arabia*
[e] *Institute of Microbiology, University of Veterinary and Animal Sciences, Lahore, Pakistan*
[f] *Department of Biomedical and Health Science Engineering, Faculty of Electrical Engineering, Universiti Teknology Malaysia, Skudai, Johor Darul Takzim, Malaysia*

ARTICLE INFO

Keywords:
Bacterial antimicrobial resistance
Silver
Nanodiamonds
Microplasma
Micro-dilution broth method
Minimum inhibition concentration

ABSTRACT

Bacterial antimicrobial resistance (BAMR) seems to pose the greatest threat to public health, food safety, and agriculture in this century. The development of novel efficient antimicrobial agents to combat bacterial infections has become a global issue. Silver nanoparticles (Ag NPs) appeared as a feasible alternative to antibiotics. However, Ag NPs face cost, toxicity, and aggregation issues which limit their antibacterial activity. This work aims to stabilize Ag NPs with enhanced antimicrobial activity at comparatively lower Ag concentrations to prevent bacterial infections. For this purpose, the Ag core was covered with nanodiamonds (NDs). Ag-NDs composite have been synthesized by microplasma technique. TEM analysis confirmed the presence of both Ag and NDs in the Ag-NDs composite. A particle size (~19 nm) was reported for Ag-NDs at the highest concentration as compared to Ag NPs (~3 nm). The conduction band of the diamond acted as an extremely strong reducing agent for Ag NPs. The large surface area of NDs stabilized the Ag NPs. A redshift (~400 nm–406 nm) in UV–visible spectra of the Ag-NDs composite indicated the formation of bigger-sized Ag NPs after incorporating NDs. XRD and LIBS analysis verified the increase in intensity of Ag-NPs by increasing ND concentration. The presence of functional groups including OH, CH, and Ag/Ag_2O was confirmed by FTIR. Bacterial inhibition growth appeared to be a dose-dependent process. The minimum inhibition concentration value of Ag-NDs composite at the highest NDs concentration against *E. coli* (~ 0.69 μg/ml) and *S. aureus* (~44 μg/ml). This is the first study to report the smallest MIC for *E. coli* (<1 μg/ml). Ag-ND composites emerged to be more efficient than Ag NPs and preferred to be used against BAMR. The enhanced antibacterial activity of the Ag-NDs composite makes it a potential candidate for antibiotics, food products, and pesticides.

* Corresponding author.
** Corresponding author.
E-mail addresses: samaniqbal.physics@pu.edu.pk (S. Iqbal), malarvili@utm.my (M.B. Malarvili).

https://doi.org/10.1016/j.heliyon.2024.e30500
Received 23 January 2024; Received in revised form 28 April 2024; Accepted 29 April 2024
Available online 3 May 2024

1. Introduction

Bacterial antimicrobial resistance (BAMR) has become a potential threat to public health, food safety, and agriculture. The genetic and physiological change in bacteria after interaction with antibiotics is known as BAMR. It is caused by unnecessary use of antibiotics, international travel, improper hygiene, and disposal of indigestible antibiotics into the ecosystem. It decreases the effectiveness of drugs against common infections and minor injuries, prolongs the hospital stay, and enhances the medical cost. Even a higher mortality rate is expected. It caused ten million deaths annually and a net worth of around 100 trillion USD to the world's economy by the end of 2050 as predicated by review [1–5]. This means drug-resistant infections resulted in more deaths than cancer. This is the worst scenario. BAMR is the point of discussion especially for underdeveloped countries. It can toxify the food at any stage during its supply. Bactericides as a pesticide play a keen role in the control of plant diseases. An estimated amount of 1.5 billion USD in crops was lost annually because of pesticide resistance only in the USA. Antibiotics are often used in food-producing animals (i.e., chickens, and cattle). A huge increase (~ 67 %) in the use of antibiotics is predicted by the end of 2030. In a previous study, traces of *Escherichia coli* (*E. coli)* were found in ground meat and inoculated milk. Humans can be easily infected with BAMR by taking contaminated food or through their interaction with animals possessing BAMR and biologicals such as blood, urine, feces, saliva, semen, etc. The world is in urgent need to address this important issue by developing a novel antimicrobial agent. The Food and Agriculture Organization, World Organization for Animal Health, and World Health Organization introduced the concept of "One Health" to address the issue of BAMR [5–7] [5–7] [5–7].

Silver (Ag) nanoparticles (NPs) have gained marvelous interest as an antiseptic and antimicrobial agent against a wide range of over 650 microorganisms which are belonging to different classes such as Gram-positive and Gram-negative bacteria, fungi and viruses including multidrug-resistant strains [1,3,8,9]. Various synthesis approaches such as physical, chemical, and biological have been utilized for Ag NP fabrication. However, high cost, long processing time, difficult experimental conditions (requirement of high pressure and temperature), and involvement of toxic chemicals limit the use of physical and chemical processes. Green synthesis is the most widely utilized process for antibacterial studies. Green synthesis offers several advantages which include feasibility, eco-friendly, cost-effectiveness, and sustainability. We are still facing issues of raw material extraction, lengthy processing time, and poor quality of the final product [10,11]. To overcome these difficulties, we must find a new synthesis approach. Microplasma glow discharge is an effective way to enhance the rate of reaction during noble metal NP synthesis. Moreover, cost-effectiveness, high electron density, surface functionalization, safety, and low processing temperature further increased its interest. Plasmas generated with water produce oxidizing or reducing agents, such as H^+, OH^-, H_2O_2, etc. The production of plasma with air could also generate N_2 and O_2 radicals which further interact with the solution. The absence of chemical reducing agents characterized the plasma electrolysis as a green process [12,13]. Mariana et al. utilized the Microplasma process for the reduction of silver nitrate salt in a sodium polyacrylate solution. Ag NPs showed efficient antimicrobial activity against *Staphylococcus aureus(S. aureus)*, *E. coli*, and *Candida albicans (C. albicans)* [12]. Muhammad et al. synthesized bimetallic gold-silver NPs using Microplasma and found an improved antiviral activity against *H9N2 influenza* [14].

However, Ag NPs still experience cost, toxicity, and aggregation issues which limit their antibacterial activity. Covering Ag NPs with a shell material is a unique way to enhance the stability, functionality, and antibacterial characteristics of Ag core [15–17]. NDs have become an object of keen interest all over the world in a broad range of applications, especially in material science and biomedicine. NDs provide excellent catalytic support to metal matrices due to their high surface area, superchemical stability, thermal conductivity, and electrical insulation required for strong metal interaction. As an excellent antioxidant agent, NDs, accelerate the electron transfer process [18,19] and can also be utilized to reduce metal salt [20]. Different scientists modified the NDs surface to enhance the reduction process and stabilize the Ag NPs using the green synthesis method [21,22]. Ag-NDs hybrid turned out to be an excellent photocatalyst against methyl blue. NDs-supported catalysts showed higher catalytic activity as compared to other commonly used materials i.e., activated carbon, graphite, or Titanium Oxide (TiO_2) [23]. The non-toxicity and biocompatibility of NDs increased their interest as efficient biosensors and biomedical carriers for delivering molecules, such as proteins, ligands, nucleic acids, antigens, and drugs into biological systems [18,19,24]. Ag-NDs composite prepared by chemical reduction method was explored as a sensitive nonenzymatic Hydrogen peroxide (H_2O_2) sensor. NDs provide a large surface area for uniform dispersion and stabilization of Ag NPs [25]. NDs have significant interest as an antibacterial material for both planktonic cells and biofilms. Antibacterial properties of NDs depend on size as well as surface functionalization (H, OH, COOH, etc.). The presence of surface groups of NDs offered benefits over other carbon-based nanomaterials due to the formation of stable water suspension and enhanced ability to link with other hydrophilic drugs [26–31] [26–31] [26–31]. NDs modified with mannose exhibited antibacterial activity against *E. coli* biofilm [27]. Amine-terminated NDs inhibited the growth and increased the mortality rate of *E. coli* on the surface of polyamide thin film [28]. Milled NDs improved the colony formation ability of *S. aureus* in deionized water [26]. Yolande et al. synthesized porphyrins functionalized Ag-NDs composite as an efficient photo-antibacterial agent for *S. aureus* planktonic cells and biofilms [32]. ND surface functionalized with menthol or cationic polymer significantly prevented *S. aureus* and *E. coli* growth [31]. Carboxylated NDs (cNDs) can penetrate the *S. mutans* cell membrane and destroy it even at MIC (minimum inhibitory concentration) of 4 μg/ml [33]. Chwalibog et al. related the zeta potential of NDs with the measured higher bacterial activity against *E. coli* and no activity against *S. aureus* [34]. Whaling et al. associated the intense antibacterial behavior against *E. coli* and *B. subtilis* with a negative charge present on the surface of NDs. However, for positively charged NDs, cell death occurred only at larger doses [35]. Ag-NDs hybrid conjugated with bovine serum albumin emerged as a potent and safe antibacterial agent against *E. coli* Bacterium. The positive activity was reported even after 36 days of treatment. However, the concentration of Ag NPs is still high (250 μgmL^{-1}) [36,37] [[,]] [36,37]. Tao et al. studied the concentration dependence of Ag-NDs composite and reported inhibition of *E. coli* growth at 6.6×10^{-4} wt% of composite in medium [38].

This work aims to stabilize Ag NPs with enhanced antimicrobial activity at comparatively lower Ag concentrations. In the present project, Ag-ND composites have been fabricated using Microplasma. The structural, morphological, optical, and antibacterial analyses were done to develop an efficient antibacterial resistance. The prepared small-size (~19 nm) nanohybrids at the highest ND concentration exhibit good antibacterial activity against *E. coli* and *S. aureus*. The reported MIC (~0.69 μg/ml) was the lowest value to inhibit *E. coli* growth up to my knowledge.

2. Materials and methods

2.1. Materials

Silver nitrate ($AgNO_3$) and Sodium dodecyl sulfate (SDS) ($NaC_{12}H_{25}SO_4$) have been purchased from Sigma-Aldrich. NDs have been synthesized using a microplasma facility. NDs with an average particle size of ~ 3 nm have been utilized in this experiment (supporting information). The details are mentioned in the literature [39].

2.2. Synthesis of Ag-NDs composite

For the fabrication of Ag-NDs composite, $AgNO_3$ (2 mM) solution was used as a precursor for Ag NPs. Different concentration of NDs ((2, 4, 8, 16) μg/ml)) were used as nanofillers. A table has been added to confirm the concentration of $AgNO_3$ and NDs used in the current work (Table 1). A 10 % SDS solution was utilized as a stabilizing agent. The $AgNO_3$ solution was slowly added to NDs and SDS aqueous solution. Finally, this solution was exposed to microplasma. A schematic and photograph of the experimental setup used for the synthesis of the Ag-NDs composite are shown in Fig. 1(a and b).

Stainless steel (SS) capillary holder and Titanium (Ti) square piece (1 cm × 1 cm) were used as cathode and anode. To achieve high electron density microplasmas, micro hollow cathode assembly was utilized. It contained five capillaries (length = 80 mm, ID = 0.5 mm and OD = 2 mm). The distance between capillaries was 2 mm. The capillary holder was placed 5 mm above the liquid solution and 3 cm away from the anode. The Argon gas was puffed through the capillaries at a flow rate of 0.2 L/min. The microplasma was ignited with a positively biased high-voltage, direct current power supply ballasted by a power resistor (1 MΩ). The discharge was operated at a constant current of 3 mA and voltage of 4 kV for 10 min. The solution was continuously stirred during the experiment to avoid aggregation of NPs. The interaction of microplasma with the electrolytic solution changed the color within a few minutes which was taken as an indication of the production of Ag -NDs composite.

For the synthesis of Ag NPs, $AgNO_3$, and SDS solution was ignited under the same microplasma condition as described above. A photograph of NDs, Ag, and Ag-NDs composite is shown in Fig. 1 (c). The incorporation of NDs changed the color of the solution from pale yellow to brownish yellow.

2.3. Characterization of Ag-NDs composite

The as-prepared Ag and Ag-NDs composites were characterized by various techniques. Transmission electron microscopy (TEM) (FEI, Morgagni, Czech Republic, accelerating voltage = 80 keV) and X-rays Diffractometer (PANalytical X'Pert PRO Diffractometer using Cu-Kα1 radiations (λ = 1.5406 A°) were used for structural analysis. The surface morphology was also examined by TEM. For TEM and XRD samples were prepared on carbon-coated grid/glass slide by drop casting method.

The Optical characterization had been investigated through UV–visible absorption (UVD-3200) spectroscopy. A LIBS 2500 plus spectrometer system (Ocean Optics Inc, USA) was used as a plasma diagnostic technique for elemental analysis. The as-prepared Ag and Ag-NDs colloidal solutions were used for optical characterization.

The functional group determination was carried out using a Fourier Transform Infrared Spectrophotometer (FT/IR-4100 type-A, Jasco). FTIR spectra were recorded by using the KBr pellet method.

For antibacterial activity, bacterial strains *E. coli* (ATCC No. 25922) and *S. aureus* (ATCC No. 25923) were taken from the Institute of Microbiology, University of Veterinary and Animal Sciences, Lahore, Pakistan. The MIC of as prepared Ag and Ag-NDs colloidal solution was found by broth microdilution method. The details of the method were described in the literature [40]. Statistical analysis was performed by Statistical Package for Social Sciences (SPSS) software using T-test. The obtained *P*-value (<0.05) confirmed the significance of the data.

Table 1
The concentration of $AgNO_3$ and NDs.

Sample	$AgNO_3$ concentration (mmol)	NDs content concentration (μg/ml)
Ag	2	0
Ag 1		2
Ag 2		4
Ag 3		8
Ag 4		16

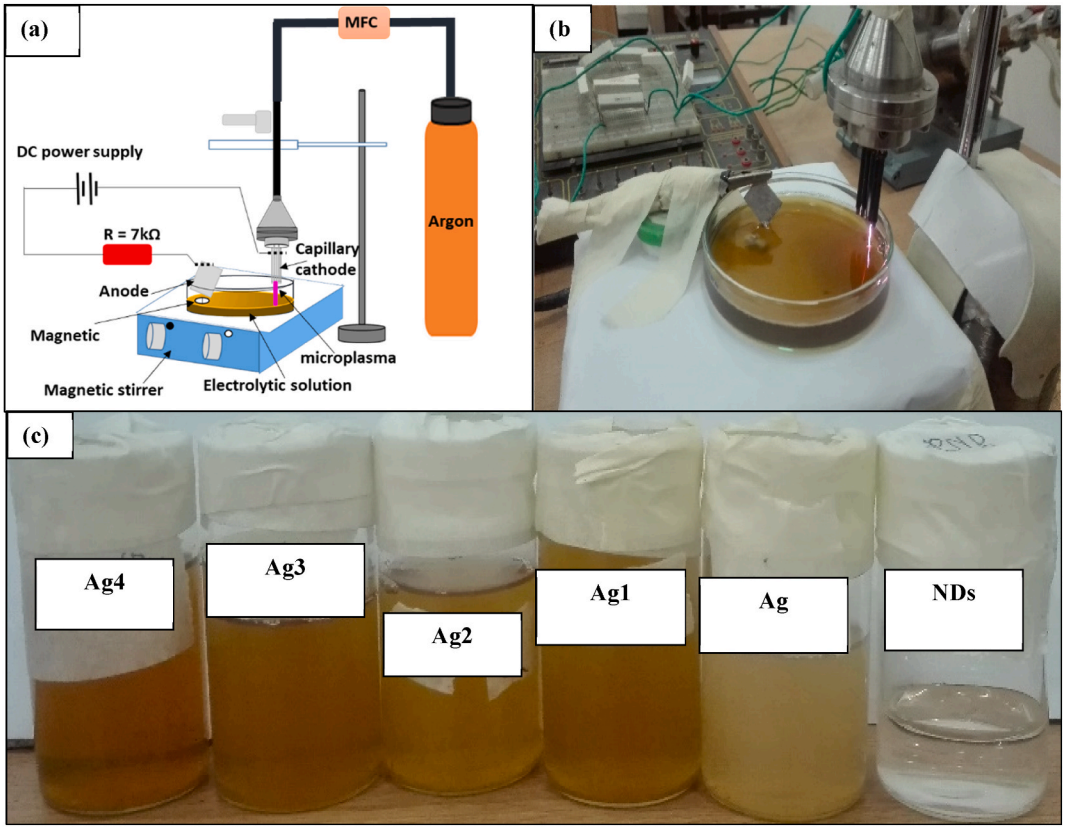

Fig. 1. A schematic (a) and photograph (b) of the experimental setup used for the fabrication of Ag -NDs composite. (c) A photograph of NDs, silver, and silver-NDs composite colloidal solution.

3. Results and discussion

3.1. TEM analysis

Fig. 2 shows the selected area electron diffraction (SAED) patterns of Ag and Ag-NDs composite at the different NDs concentrations. TEM analysis of NDs is shown in Fig. S1 (supporting information).

SAED pattern reflects the crystallinity of Ag (Fig. 2 a). The bright rings along with the spot confirm the (111), (200), (220), (311), and (222) planes of Ag NPs. The d-spacing is assigned to the cubic silver (JCPDS No 04–0783) [41]. Fig. 2 (b) represents the SAED patterns on the Ag-NDs composite confirming the multiple crystal diffraction features of Ag and NDs. The bright circular rings along with the spot not only correspond to silver but also (100), (002), (101), and (102) planes of diamond. The calculated interplanar distances are matched with Lonsdaleite diamond (JCPDS No 19–0268) [39,42,43] [[,]] [39,42,43] [[,]] [39,42,43]. The small carbon

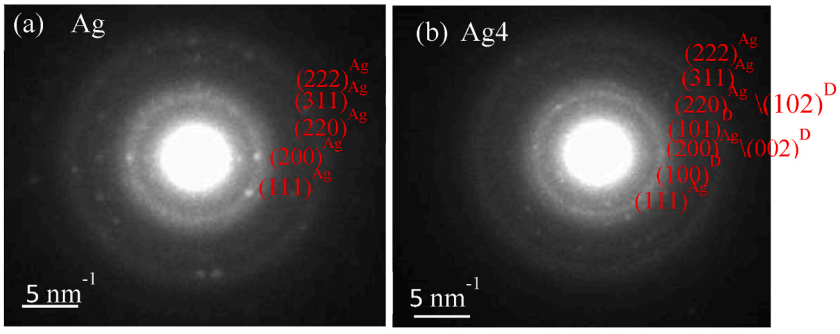

Fig. 2. SAED patterns of Ag NPs (a) and (b–e) Ag-NDs at different NDs concentrations. where, Agi = Ag matrix at different ND concentrations, where D = diamond and Ag = silver.

fraction and density contrast between silver and carbon make difficult the observation of the carbon phase in this sample [44]. The lattice d-spacing of rings calculated from SEAD data is described in Table 2. The strong interaction between NDs and Ag improves the bonding and crystallinity of Ag.

Fig. 3 presents the TEM images of Ag NPs (Fig. 3 a), and Ag-NDs composite (Fig. 3 (c, e, g, i)). According to the literature, Ag NPs are prone to exist in the spherical form [17] as confirmed by Fig. 3(a). The addition of NDs resulted in the quasi-spherical shape of the Ag-NDs composite. Particle size distribution is seen (Fig. 3 (b, d, f, h, j)) as a histogram of Ag-NDs composites at different NDs concentrations. The average particle size and particle size distribution of NPs were estimated by using Image J software. The particle size of Ag NPs ranges from 1 to 11 nm (Fig. 3(b)). The average particle size is ~3 nm. Fig. 3 (i) reveals the TEM images of Ag- NDs composite at the highest concentration. The average particle size is estimated to be ~ 19 nm. Overall, an enhancement in particle size is observed.

A proposed redox reaction is described in supporting information. The interfacial chemical reactions and particle transport mechanism are responsible for the size and growth of NPs [9]. Ag NPs and Ag-NDs composite were synthesized by microplasma liquid interaction. Plasmas generated with water produce oxidizing or reducing agents through electron impact dissociation. Moreover, the experiment in the air could also generate N_2 and O_2 radicals which further interact with the solution. Highly reactive species are responsible for the reduction of metal cations [45]. Initially formed Ag NPs provide nucleation seed. The addition of NDs accelerates the catalytic Ag^+ ion reduction, consequently, Ag/Ag_2O NPs are formed and particle size increases [9,20]. The conduction band of the diamond acted as an extremely strong reducing agent for Ag NPs. For higher ND concentrations, rapid reduction stimulates a fast nucleation rate which results in a large number of relatively small NP formations. Small-sized particles tend to aggregate. Because small particle size acquires larger surface energy and induces destabilization in the system. Growth (Ostwald ripening) of particles is a mass transfer phenomenon. During this process, NPs with a higher collision frequency of nucleated particles lead towards their aggregation into bigger-sized NPs. Aggregation of NPs lowers its surface energy and stabilizes the system [9,20]. Light edges as compared to the center of NPs confirmed the capping of Ag with NDs. TEM analysis did not allow the identification of oxide species in the NPs [17]. It is not surprising to observe a small amount of Ag_2O alongside Ag NPs. It is consistent with earlier research work [46]. The presence of Ag_2O strongly depends on the synthesis technique and experimental conditions [46,47]. A pictorial representation of the proposed mechanism of Ag-NDs composite formation is shown in Fig. S2.

Reducing agents and stabilizers are important factors to control the morphology of NPs. In this research work, SDS is used as an electrostatic stabilizer. The Ag+ion interacts with the hydrophilic headgroup (OSO_3^-) of SDS. The Ag + ions were reduced by NDs and microplasma (as described above). SDS acts as a protecting agent to avoid the agglomeration of NPs.

3.2. UV–visible spectroscopy analysis

Fig. 4 (a) illustrates the UV–visible spectra of Ag and Ag-NDs composite at different ND concentrations. A single surface plasmon resonance (SPR) indicates the formation of spherical particles as confirmed by TEM analysis (Fig. 3). The SPR peak of Ag NPs was found at ~400 nm [48]. The appearance of only one absorbance band of Ag NDs composite indicates homogeneously mixed colloidal particles without significant formation of independent particles [49]. The decrease in intensity and shifting of SPR towards a higher wavelength (~406 nm) is observed at lower ND content. This is spectroscopic evidence of the presence of NDs along with Ag NPs. The shifting indicates the comparatively bigger size of the composite as compared to Ag NPs and confirms the chemical interaction between Ag and NDs composite as discussed earlier in TEM analysis (Fig. 3). The lower concentration of NDs is responsible for the absence of a diamond absorption band and implies the enrichment of Ag atoms in the nanocomposite [50]. From the UV–visible spectra, we can sensibly interpret that the reduction of Ag salt alone occurs on the NDs surface instead of forming new nucleation sites, the core-shell structure of Ag-NDs composite is formed. Thus, it is not astonishing that the optical properties of the composite are dominated by the silver and the plasmon band of the composite redshifts with increasing ND concentration [49]. A general trend of this spectra is that the peaks increased and shifted to the right (at the highest NDs concentration), which means that the NDs encapsulate Ag NPs [51]. The reduction of silver ions increases the number of Ag NPs in the aqueous solution and results in an enhancement in the intensity of spectra. It can also be taken as evidence for the stabilization of Ag NPs after NDs incorporation.

Table 2
d-spacing measured from SEAD pattern.

Sample	*hkl*	Calculated d-spacing (nm)
Ag	$(111)^{Ag}$	2.32
	$(200)^{Ag}$	2.02
	$(220)^{Ag}$	1.46
	$(311)^{Ag}$	1.26
	$(222)^{Ag}$	1.16
Ag4	$(111)^{Ag}$	2.36
	$(100)^{D}$	2.20
	$(200)^{Ag}/(002)^{D}$	2.04
	$(101)^{D}$	1.92
	$(220)^{Ag}/(102)^{D}$	1.46
	$(311)^{Ag}$	1.25
	$(222)^{Ag}$	1.18

*Where, Ag= Silver, D = Lonsdaleite diamond.

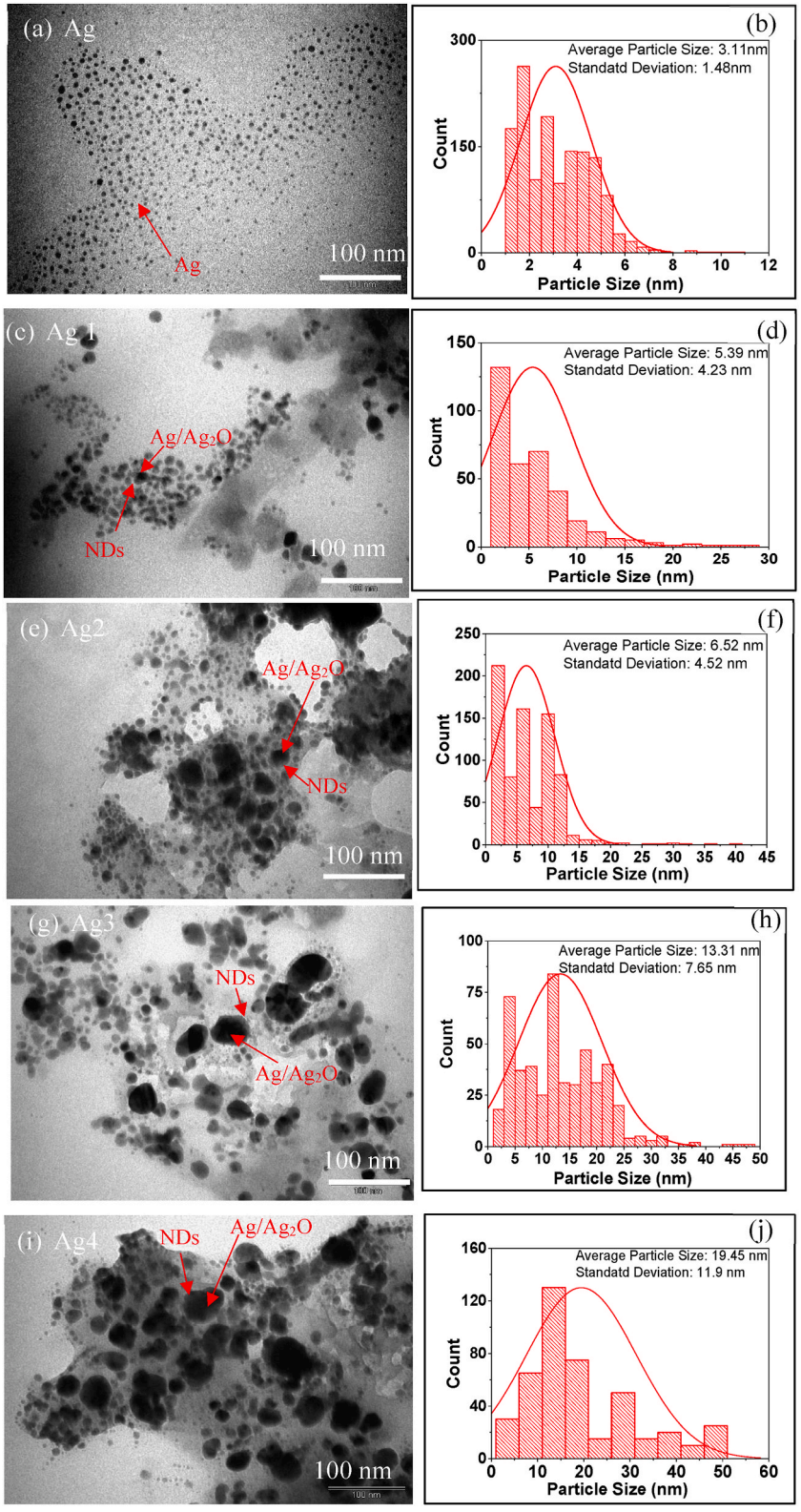

Fig. 3. TEM images of (a) Ag NPs and (c, e, g, i) Ag NDs composite at different NDs concentrations. Where, Agi = Ag matrix at different NDs concentration, (b, d, f, h, j) histogram representing particle size distribution. Arrows are marked for identification of Ag/Ag_2O and NDs.

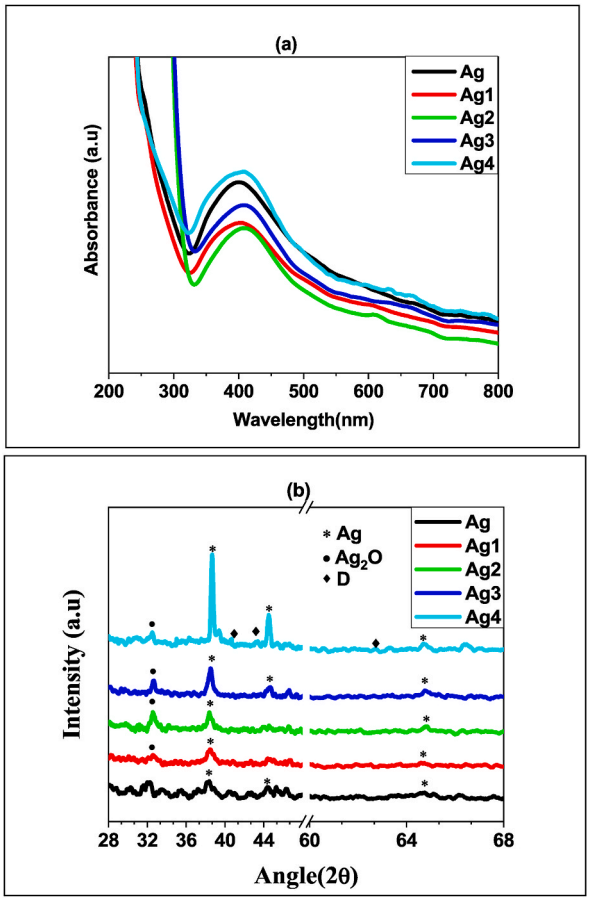

Fig. 4. (a) UV Visible spectra of Ag-NDs composite at different NDs concentrations. (b) XRD patterns of Ag- NDs composite at different NDs concentration where, Agi = Ag matrix at different NDs concentration.

Table 3
XRD data of Ag-NDs composite at different NDs concentration.

Sample	Angle (2θ)	Nature of NPs	Plane	FWHM (θ)	d-spacing (nm)	Grain size (nm)	Stress
Ag	38.23	Ag	111	0.768	2.35	10.9	0
	44.42	Ag	200	0.925	2.03	9.28	−0.0049
	64.57	Ag	220	0.462	1.44	20.3	0
Ag1	32.64	Ag_2O	111	0.944	2.74	8.77	0.0073
	38.46	Ag	111	0.787	2.34	10.7	−0.0042
	64.67	Ag	220	0.683	1.44	13.8	0
Ag2	32.55	Ag_2O	111	0.912	2.74	9.07	0.0073
	38.45	Ag	111	0.762	2.34	11.1	−0.0042
	64.81	Ag	220	0.403	1.43	23.2	−0.0069
Ag3	32.63	Ag_2O	111	0.472	2.74	17.5	0
	38.51	Ag	111	0.393	2.34	21.4	−0.0042
	44.51	Ag	200	0.576	2.03	14.9	−0.0049
	64.82	Ag	220	0.401	1.43	23.5	−0.0069
Ag4	32.48	Ag_2O	111	0.357	2.75	23.2	0.0073
	38.61	Ag	111	0.059	2.33	144	−0.0098
	40.7	D	100	0.266	2.21	31.8	0.0091
	43.28	D	002	0.335	2.08	25.5	0.0097
	62.7	D	102	0.98	1.48	9.49	−0.0133
	44.42	Ag	200	0.384	2.03	22.3	−0.0049
	64.68	Ag	220	0.691	1.44	19.2	0

3.3. XRD analysis

Fig. 4 (b) shows the XRD patterns on the Ag-NDs composite at different ND concentrations. The Ag NPs have a polycrystalline crystal structure. The XRD reflections of (111), (200), and (220) can be assigned to cubic silver (JCPDS No 04–0783) confirming the formation of Ag NPs colloidal. After the introduction of NDs, a slight shift and broadening in (111) reflection with the appearance of (111) reflection of silver oxide was observed. The (111) diffraction planes of cubic silver oxide, Ag_2O, (JCPDS No 41–1104). Furthermore, small peaks around (100), (002), and (102) associated with Lonsdaleite diamond (JCPDS No 19–0268) were observed. The lower content of NDs or strong diffraction signals of silver suppresses the diffraction of NDs [52,53].

Silver is extensively heavier than oxygen and can be readily oxidized by atmospheric oxygen. Oxidation takes place entirely near the surface of the NPs which decreases the oxidation potential of Ag^+/Ag [44]. A proposed mechanism for the formation of Ag/Ag_2O might be related to the dissociation of $AgNO_3$ into silver oxide. The aqueous vapor atmosphere supports a stoichiometric relation with Ag^{1+} rather than Ag^{2+}, which requires an oxygen-deficient environment [54]. It was assumed that Ag_2O formation occurs as a fellow, $2Ag^+ + OH^- \rightarrow Ag_2O$ [55]. There is a strong tendency of metallic Ag clusters and Ag_2O transformation to Ag NPs as observed from XRD. The increase in peak intensity with ND concentrations indicates the good crystallinity and stabilization of Ag NPs [48].

It might also be proposed that at low NDs concentrations, some of the silver reacts with atmospheric oxygen or with water to produce silver oxide on the surface of NDs. Thus, NDs help to reduce silver in a low potential state such as silver oxide (Ag_2O). Oxide formation results in shrinkage of the silver core, which in turn affects the SPR of Ag (as confirmed by UV visible). By increasing the NDs concentration, the strong interaction between NDs and Ag improves the bonding and crystallinity of silver as reported here. NDs act as strong reducing agents for the reduction of silver ions to silver NPs. Thus, stable Ag NPs are observed at the cost of Ag_2O.

The concentration of the capping agent is an important factor in controlling the Ag NP size [56]. In the small amount of stabilizer, all the silver atoms cannot form coordination bonds with the stabilizer. Thus, the detection of silver oxide diffraction peaks in composite might be related to the SDS caped layer on Ag NPs which is not able to prevent it from oxidation [57].

The XRD data is given in Table 3. A sharp increase in crystalline size indicates an improvement in overall crystallinity. The calculated value of stress indicates the compressive nature which shifts the peak towards a higher angle as compared to bulk. This peak

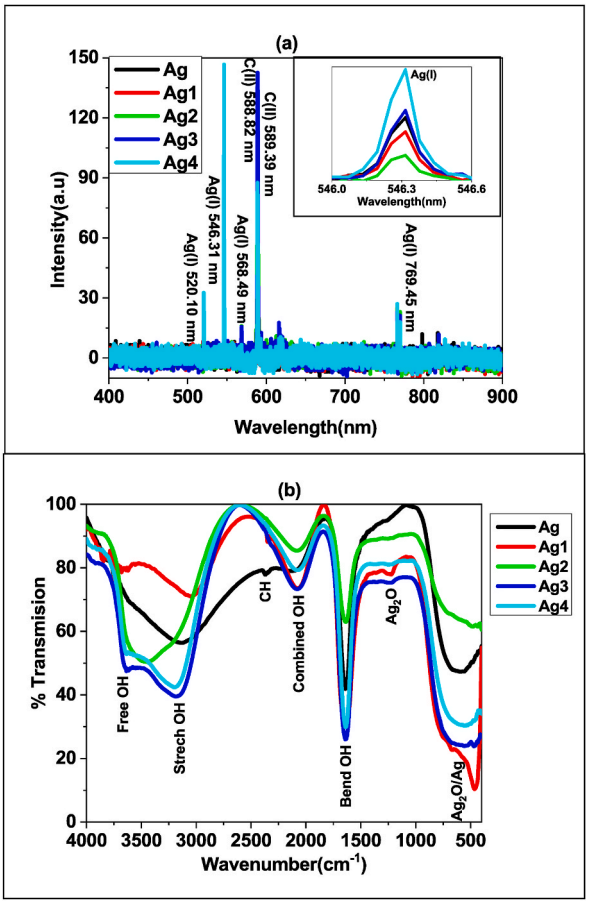

Fig. 5. (a) LIBS spectra of Ag-NDs at different NDs concentrations. Inset is an enlarged image of LIBS spectra at Ag(I) at 546.31 nm wavelength. (b) FTIR spectra of Ag-NDs composite at different NDs concentrations. where, Agi = Ag matrix at different NDs concentration.

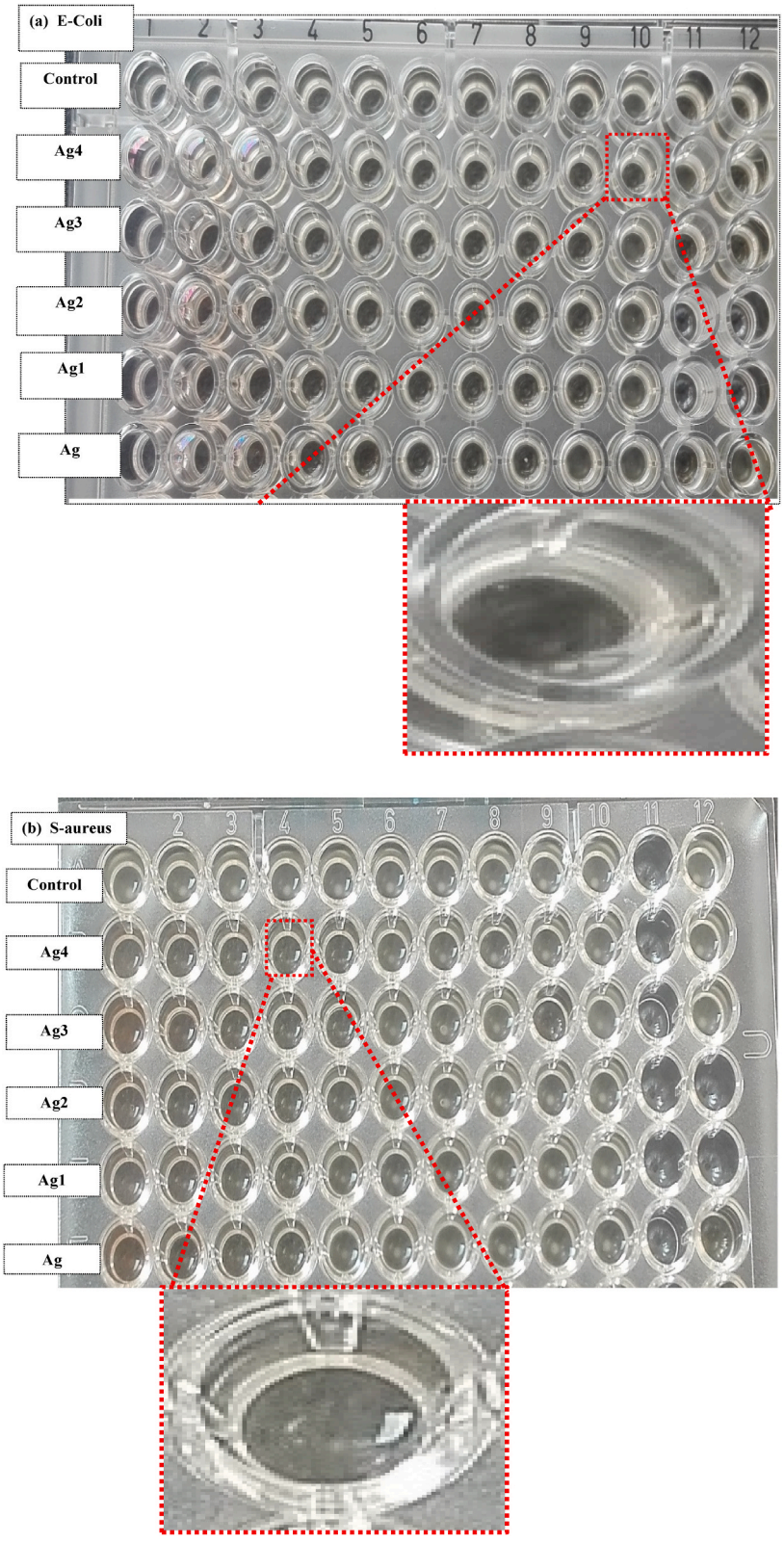

Fig. 6. A panel of 96 well plates array with Ag-NDs composite at different NDs concentration (where, Agi = Ag matrix at different NDs concentration) for (a)*E-coli* and (b) *S- aureus*. The enlarged image is Ag- NDs composite with the lowest value of MIC (minimum inhibition concentration).

shifting highlighted the nanoscale nature of silver and resulted in lattice compression due to surface stresses [58].

3.4. LIBS analysis

Fig. 5(a) shows the LIBS (Laser-Induced Breakdown Spectroscopy) spectra of Ag-NDs composite at different NDs concentrations. Inset is the enlarged image of LIBS spectra exhibiting the intensity variation of Ag (I) at 546.31 nm wavelength. Four spectral lines of silver, Ag (I) 520.10 nm, Ag (I) 546.31 nm, Ag (I) 568.49 nm and Ag (I) 769.45 nm were detected and labeled in LIBS spectra. These lines are present in all LIBS spectra without and with NDs [59]. The presence of diamond is taken from carbon emission lines, C (II) 588.82 nm and C (II) 589.39 nm [60]. These lines are also confirmed by the NIST database. To evaluate the effect of NDs concentration on Ag-NDs composite, one takes the maximum intense peak of silver, Ag(I) 546.31 as shown in the inset in Fig. 5(a). An initial decrease in Ag ion intensity is observed with ND concentrations. However, a further increase in ND concentration increases the Ag intensity by improving the strong interaction between NDs and Ag. These results are consistent with TEM and XRD analysis (Fig. 4 (b)).

3.5. FTIR analysis

The FTIR spectra are shown in Fig. 5(b). The most prominent band ~3200 cm^{-1} and 1640 cm^{-1} belong to the stretching and bending vibrations of the OH group. The band ~2080 cm^{-1} (only observed in composite) is related to the coupling of OH bands [61]. Addition peaks (~3700 cm^{-1}) belong to free hydroxyl groups which are found only at higher ND concentrations [62]. The CH band is found at ~2335 cm^{-1}. The small shift and alteration in Band shape or intensity prominent in the composite are attributed to the interaction of NDs with Ag NPs. The metal carbonate complex band ~ 1249 cm^{-1} confirms the formation of Ag_2O compounds [48]. The presence of the Ag/Ag_2O NPs is confirmed from the band around 500-600 cm^{-1} [61,63]. Shifting of the OH band (3213-3283 cm^{-1}) towards a higher wavenumber indicated the enhancement of particle size as confirmed by TEM and UV–visible spectroscopy analysis. It is assumed that NDs stabilized the Ag NPs by electrostatic interaction of positively charged Ag ion and negatively charged OH group. Oxygen from the OH group donates electrons to $(Ag^0)_n$ or Ag_2O for the reduction of Ag^+ ion and results in bigger Ag clusters [55].

3.6. Antibacterial activity

The results of the microdilution broth method for Ag-NDs composite against Gram-negative bacteria (*E. coli*) and Gram-positive bacteria (*S. aureus*) are shown in Fig. 6 (a, b). The first row is assigned to control, without any antibiotic. Ag-NDs composite with different ND concentrations are arranged from the second to the sixth row. Ag NPs as well as Ag-NDs composite show antibacterial activity against both gram-positive and gram-negative bacteria.

The MIC is found by counting the well of specific Ag-NDs composite's concentration with negative antibacterial activity. As the concentration of Ag is fixed, the minimum concentration of NDs for bacterial inhibition is to be explored. The relationship between MIC and Ag-NDs composite is summarized in Fig. 7.

Ag-NDs composite at lower NDs concentration (~ 8 μg/ml) show similar anti-bacterial activity as that of Ag NPs. However, the highest concentration of NDs (~ 16 μg/ml) in Ag-NDs composite exhibits efficient antibacterial activity as compared to Ag NPs for both gram-positive and gram-negative bacteria. Antibacterial activity appeared to be a concentration-dependent process as reported earlier, lower concentrations (5 μg/ml) of NDs prevent only 25 % growth of bacteria. However, a ten times enhancement in concentration resulted in 100 % growth inhibition [35].

The improved antibacterial activity of Ag-NDs is attributed to the contribution of both NDs and Ag/Ag_2O in antibacterial activity.

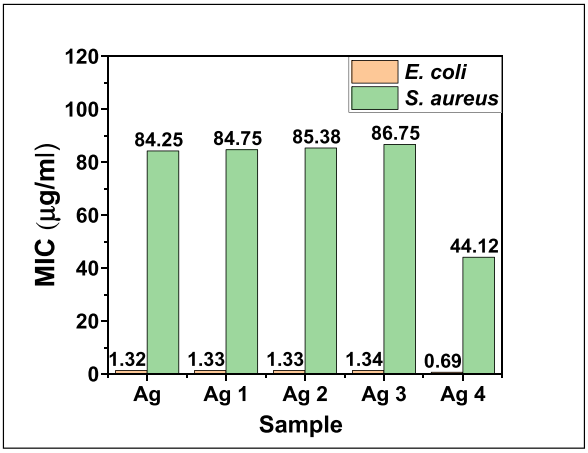

Fig. 7. MIC (minimum inhibition concentration) value of Ag- NDs composite at different NDs concentration (μg/mL) against *S-aureus* and *E-coli*.

Table 4
Antibacterial activity of Ag NPs, Ag_2O NPs and Ag composite.

Sr no	Synthesis methods	Type of NPs	Average particle Size (nm)	Antibacterial test	Bacterial strain	Results	Reference
1	Green synthesis (Euphorbiaceae leaves)	Ag	~9-20	Broth microdilution technique	*E. coli* (ATCC 25922) **P.aeruginosa* (ATCC 27852) *S. aureus* (ATCC 25923) **E. faecalis* (ATCC 27852)	MIC = 4 μg/ml MIC = 8 μg/ml MIC = 16 μg/ml MIC = 32 μg/ml	[68]
2	Green synthesis (Entada. spiralis stem)	Ag	~17–19	Disk diffusion method	*E. coli* (ATCC 25923) **P. vulgaris* (ATCC 33420) *S. aureus* (ATCC 25922) **E. faecalis* (ATCC 29212)	~ 7.97 ± 0.17 mm ~8.34 ± 0.11 mm ~10.47 ± 0.37 mm ~ 8.41 ± 0.17 mm *(for E. spiralis-Ag NPs = 40 μg/ml)*	[69]
3	Green synthesis (Bromelain)	Ag	~7–24	Broth microdilution technique	*E. coli* (ATCC 11229) *S. aureus* (ATCC 25923)	MIC = 8 μg/ml MIC = 4 μg/ml	[16]
4	Green synthesis (Paeoniaemodi leaves)	Ag_2O	38–86	Well diffusion method	*E. coli* **P.aeruginosa* *S. aureus* **B. subtilis*	4.231 mm 2.609 mm 2.276 mm 2.267 mm (for 60 μl Ag-NPs)	[63]
5	Green synthesis (*E. odoratum* leaves)	Ag/Ag2O	23	Broth microdilution technique	*E. coli* **S. typhi* *S. aureus* **B. subtilis*	MIC = 25 μg/ml MIC = 40 μg/ml MIC = 75 μg/ml MIC = 75 μg/ml	[65]
6	Green synthesis Rutin extract	Ag- mesoporous silica	155–188	Broth microdilution technique	*E. coli* (ATCC 11229) *S. aureus* (ATCC 25923)	MIC = 4.2 μg/ml MIC = 6.25 μg/ml *(For 10 % Ag loading)*	[66]
7	Green synthesis (Opuntia fcus indica)	ZnO@ Ag@Au	~800	Well diffusion method	*E. coli* **P.aeruginosa* *S. aureus* **B. subtilis*	18 mm 19 mm 18 mm 15 mm *(ZnO@Ag@Au = 60 μg/ml)*	[64]
8	microwave irradiation	Ag containing fluorapatite	~69	Disk diffusion method	*E. coli* *S. aureus*	1.25 cm 0.85 cm *(Ag = 0.3 wt %, F = 1.9 wt %)*	[67]
9	Physical adsorption	Ag- NDs@ bovine serum albumin	100–200	Broth microdilution technique	*E. coli (*strain K12 MG1655*)*	MIC = 250 μg/ml *(after 36 days)*	[37]
10	In situ reduction/ deposition	Ag@NDs	100	Optical density-600nm	*E. coli* (ATCC 25922)	No absorbance *(6.6×10^{-4} wt% of Ag@NDs)*	[38]
11	Physical mixing	GO@Ag	100–3000	Well diffusion method	**P.aeruginosa* (ATCC 27852) *S. aureus* (ATCC 25923)	~ 28 ± 0.4 mm ~ 23 ± 1.6 mm (AgNP = 25 μg/ml, GO = 10 μg/ml)	[70]
12	Liquid-liquid intwrfacial precepitation	Ag–C60	Not mentioned	Spread plate method	*S. aureus* (ATCC 29213)	88.98 % = light irradiation for 20 min 19.05 % = dark	[71]
13	Microplasma	Ag@NDs	19	Broth microdilution technique	*E. coli* (ATCC 25922) *S. aureus* (ATCC 25923)	0.69 μg/ml 44.13 μg/ml (for Ag NPs = 2 mmol, NDs = 16 μg/ml)	This work

**P. aeruginosa* = *Pseudomonas aeruginosa*, * *E. faecalis* = *Enterococcus faecalis*, **S. typhi* = *Salmonella typhi* *Proteus vulgaris = P. Vulgaris, *B. subtilis = Bacillus subtilis, *S. paratyphi = Salmonella paratyphi.

Table 4 describes the antibacterial properties of Ag, Ag_2O, and Ag- composite [64–71] [64–71] [64–71]. Ag NPs individually as well as in composite form exhibit excellent antibacterial activity. Ag_2O also emerged as an outstanding antimicrobial agent against 53 species (21 g-positive, 15 g-negative, 17 fungal) [72]. A proposed mechanism of Ag/Ag_2O is described below. According to the literature [8,9,16,48,72], Ag^+ ions and Ag^0 released from Ag/Ag_2O NPs directly damage cell wall integrity by binding, accumulating, or penetrating inside the cell wall and cytoplasmic membrane. The interaction of Ag^+ ions with sulfur and phosphorus-containing compounds such as proteins, and DNA disturb cell functions. The adherence of Ag^+ ions and reactive oxygen species to the deoxyribonucleic acid prevents

DNA duplication, resulting in loss of cell viability and leading to cell death. A modification in cell membrane charge and permeability is also reported due to the attachment of silver ions to the cell wall. This phenomenon is often related to antifungal activity. In another approach, the interaction of Ag ions with thiol groups of enzymes, such as NADH dehydrogenases, disturb the respiratory chains, prevent ATP (adenosine triphosphate) production, imbalance the energy cycle, improves the reactive oxygen species (ROS) synthesis, and finally generate oxidative stress. Ag NPs may also produce free radicals which induce oxidative stress for cell membrane destruction. Moreover, Ag_2O also releases oxygen which is beneficial for antibacterial activity. Interestingly, photocatalytic activity is the last proposed mechanism that enhanced the attachment of Ag/Ag_2O NPs to drugs [8,9,16,48,72]. It was known that smaller Ag NPs (<10 nm) exhibit higher antibacterial activity. However, the optimized size of Ag NPs (<30 nm) was reported for *S. aureus* and *Klebsiella pneumoniae* [12,36], [12,36]. In current research work, the largest particle size of the as-synthesized Ag-NDs composite (~19 nm) was still smaller than the optimized value required for bacterial growth inhibition.

The development of new antibiotics is a costly and time-consuming process. We must verify the safety and efficiency of the drug for years before final approval by the drug regulatory authority. However, antimicrobial-resistant bacteria keep on growing and causing infections/deaths during this period. Therefore, in this defined post-antibiotic era, Ag NPs along with other nanomaterials emerge as exceptional alternatives to inhibit pathogenic microorganisms at comparatively lower Ag NP doses without the development of new resistance [73]. Carbon-based nanomaterials (CNMs) especially Nanodiamonds (NDs) and Graphene derivatives (GD) [Graphene, graphene oxide, Graphene NPs, and reduced graphene] have been extensively utilized as a vital antibacterial agent. Even though CNMs could not show any visible activity. But they act as an efficient carrier for Ag NPs. Ag-GD composites become an eminent antibacterial agent against *E. coli, S. aureus*, and *Pseudomonas aeruginosa* (*P. aeruginosa)* [74,75]. Antibacterial properties of NDs depend on size as well as surface functionalization (OH, H, COOH, etc.) [26–31] [26–31] [26–31]. The synthesized NDs (~3 nm) with a functional group (-OH) improve the performance of the Ag- composite. NDs act as a reservoir for Ag/Ag_2O NPs and control the release of Ag^+ ions/Ag^0. It was assumed that NDs show significant antibacterial activity against *E. coli* by surrounding and destroying cell walls [29]. Membrane leakage is also considered one of the mechanisms that produce pores to allow ROS in the cell (*S. aureus* and *E. coli*) and cause oxidative damage to DNA or proteins [31]. Some researchers relate the antibacterial activity of NDs to the presence of a negative charge associated with the acid anhydride group [27,28] [[,]] [27,28]. NDs also improved the photocatalytic activity of Ag NPs [23]. Thus, in Ag-NDs composite, NDs disrupt the cell membrane and facilitate the transport of Ag^+ ions across the cell membrane.

The Ag-NDs composites exhibit higher antibacterial activity towards *E. coli* compared to *S. aureus* (Fig. 7) as predicted from earlier work [12,68]. The thicker peptidoglycan layer of *S. aureus* requires more concentration of Ag-NDs composites than *E. coli* [48]. Moreover, the outer cell wall of *E. coli* contains a negatively charged lipopolysaccharide layer capable of attaching even a weak positive charge present on the surface of Ag NPs [76]. This difference in dose for both bacteria indicate the influence of concentration on antibacterial activity. The increasing concentration of NDs accelerates the diminishing of bacteria.

These are our preliminary results confirming the concentration dependence antibacterial activity of Ag-NDs. To understand the exact mechanism, we have a plan to check the dependency of antibacterial rate and cytotoxicity on different bacterial strains, size, and concentration of nanoparticles in the future. The mode of interaction will be confirmed further by electron microscopy and confocal microscopy. Previously, NDs have been explored as an efficient antibacterial agent in the form of particles, coating, and composite. They can act as a carrier for other materials (silver) and be dispersed in the biological medium [34]. Microplasma-synthesized NDs exhibit excellent antibacterial activity and report the lowest MIC against *E. coli* (<1 μg/ml) up to my knowledge. Inhabitation of bacterial growth is an outstanding property for antibiotics, food products, and pesticides.

4. Conclusions

Microplasma technique has been used for the synthesis of Ag NPs and Ag-NDs. An increase in grain (~144 nm) and particle size (~19 nm) is observed in Ag-NDs composite as compared to Ag. Both Ag and Ag-NDs composites exhibit antibacterial activity towards *E. coli* and *S. aureus*. The cell membrane penetrating properties and the oxidative stress of NDs/Ag and free radical formation of Ag NPs collectively contribute to enhancement in the antibacterial efficacy of Ag-NDs-composite as compared to Ag alone. Bacterial inhibition growth appeared to be a dose-dependent process. The increasing concentration of NDs accelerates the diminishing of bacteria. The interaction of Ag-NDs also depends on the cell wall of bacteria. *S. aureus* required a higher MIC value as compared to *E. coli.* The MIC value of Ag-NDs composite at the highest NDs concentration against *E. coli* (~ 0.69 μg/ml) and *S. aureus* (~44 μg/ml). This is the first study to report the smallest MIC for *E. coli* (<1 μg/ml). Thus, one concludes that Ag-ND composites are more efficient than Ag NPs and preferred to be used against BAMR in antibiotics, food products, and pesticides.

Data availability

The experimental datasets obtained from this research work and then the analyzed results during the current study are available from the corresponding author upon reasonable request.

CRediT authorship contribution statement

Saman Iqbal: Writing – review & editing, Writing – original draft, Methodology, Investigation, Formal analysis, Conceptualization. **Muhammad Shahid Rafique:** Supervision, Conceptualization. **Nida Iqbal:** Writing – review & editing, Methodology. **Sultan Akhtar:** Esources, Software. **Aftab Ahmad Anjum:** Resources. **M.B. Malarvili:** Writing – review & editing.

Declaration of competing interest

The authors declare that they have no known competing financial interests or personal relationships that could have appeared to influence the work reported in this paper.

Appendix A. Supplementary data

Supplementary data to this article can be found online at https://doi.org/10.1016/j.heliyon.2024.e30500.

References

[1] A.Y. Yakoup, A.G. Kamel, Y. Elbermawy, A.S. Abdelsattar, A. El-Shibiny, Characterization, antibacterial, and cytotoxic activities of silver nanoparticles using the whole biofilm layer as a macromolecule in biosynthesis, Sci. Rep. 14 (2024) 364, https://doi.org/10.1038/s41598-023-50548-9.

[2] N. Bano, D. Iqbal, A. Al Othaim, M. Kamal, H.M. Albadrani, N.A. Algehainy, H. Alyenbaawi, F. Alghofaili, M. Amir, Roohi, Antibacterial efficacy of synthesized silver nanoparticles of Microbacterium proteolyticum LA2(R) and Streptomyces rochei LA2(O) against biofilm forming meningitis causing microbes, Sci. Rep. 13 (2023) 4150, https://doi.org/10.1038/s41598-023-30215-9.

[3] G. Waktole, B. Chala, The role of biosynthesized metallic and metal oxide nanoparticles in combating anti-Microbial drug Resilient pathogens, J. Biomaterials Nanobiotechnol. 14 (2023) 1–22.

[4] M.M. Aljeldah, M.T. Yassin, A.A.-F. Mostafa, M.A.M. Aboul-Soud, Synergistic antibacterial potential of greenly synthesized silver nanoparticles with fosfomycin against some nosocomial bacterial pathogens, Infect. Drug Resist. (2023) 125–142.

[5] P. Yadav, M. Singhal, S. Chatterjee, S. Nimesh, N. Gupta, Grewia tenax-mediated silver nanoparticles as efficient antibacterial and antifungal agents, Nanomater. Nanotechnol. 2024 (2024) 9912599, https://doi.org/10.1155/2024/9912599.

[6] M. Samtiya, K.R. Matthews, T. Dhewa, A.K. Puniya, Antimicrobial resistance in the food chain: trends, mechanisms, pathways, and possible regulation strategies, Foods 11 (2022) 2966.

[7] S.A. Miller, J.P. Ferreira, J.T. LeJeune, Antimicrobial use and resistance in plant agriculture: a one health perspective, Agriculture 12 (2022) 289.

[8] A. Wasilewska, U. Klekotka, M. Zambrzycka, G. Zambrowski, I. Święcicka, B. Kalska-Szostko, Physico-chemical properties and antimicrobial activity of silver nanoparticles fabricated by green synthesis, Food Chem. 400 (2023) 133960, https://doi.org/10.1016/j.foodchem.2022.133960.

[9] S. Gevorgyan, R. Schubert, S. Falke, K. Lorenzen, K. Trchounian, C. Betzel, Structural characterization and antibacterial activity of silver nanoparticles synthesized using a low-molecular-weight Royal Jelly extract, Sci. Rep. 12 (2022) 14077, https://doi.org/10.1038/s41598-022-17929-y.

[10] S. Ying, Z. Guan, P.C. Ofoegbu, P. Clubb, C. Rico, F. He, J. Hong, Green synthesis of nanoparticles: current developments and limitations, Environ. Technol. Innov. 26 (2022) 102336, https://doi.org/10.1016/j.eti.2022.102336.

[11] K.M. Mahmud, MdM. Hossain, S.A. Polash, M. Takikawa, M.S. Shakil, M.F. Uddin, M. Alam, M.M. Ali Khan Shawan, T. Saha, S. Takeoka, MdA. Hasan, S. R. Sarker, Investigation of antimicrobial activity and biocompatibility of biogenic silver nanoparticles synthesized using syzigyum cymosum extract, ACS Omega 7 (2022) 27216–27229, https://doi.org/10.1021/acsomega.2c01922.

[12] M. Shepida, O. Kuntyi, Y. Sukhatskiy, A. Mazur, M. Sozanskyi, Microplasma synthesis of antibacterial active silver nanoparticles in sodium polyacrylate solutions, Bioinorgan. Chem. Appl. 2021 (2021).

[13] D. Mariotti, R.M. Sankaran, Perspectives on atmospheric-pressure plasmas for nanofabrication, J. Phys. D Appl. Phys. 44 (2011) 174023.

[14] M. Zubair, M.S. Rafique, A. Khalid, T. Yaqub, M.F. Shahid, S.Y. Alomar, M.A. Shar, The fabrication of gold–silver bimetallic colloids by microplasma: a worthwhile strategy for counteracting the surface activity of avian influenza virus, Crystals 13 (2023) 340.

[15] J. Cui, M. Wan, Z. Wang, Y. Zhao, L. Sun, Preparation of PAN/SiO2/CTAB electrospun nanofibrous membranes for highly efficient air filtration and sterilization, Sep. Purif. Technol. 321 (2023) 124270, https://doi.org/10.1016/j.seppur.2023.124270.

[16] F. Gheisari, S. Reza Kasaee, P. Mohamadian, S. Chelliapan, R. Gholizadeh, Z. Zareshahrabadi, S. Pooria Solhjoo, E. Vafa, S. Mosleh-Shirazi, A. Mohammad Amani, H. Kamyab, Bromelain-loaded silver nanoparticles: formulation, characterization and biological activity, Inorg. Chem. Commun. 161 (2024) 112006, https://doi.org/10.1016/j.inoche.2023.112006.

[17] V. de C.G. Videira, B.N. Harada, V.G. Vital, R.A.G. da Silva, S.P. de Vasconcellos, D.S. Pellosi, Structural and antibacterial evaluation of copper, silver, and bimetallic silver/copper nanoalloys synthesized in chitosan biopolymer, Materials 3 (2024) 100071, https://doi.org/10.1016/j.nxmate.2023.100071.

[18] T. Chen, X. Tian, L. Huang, J. Xiao, G. Yang, Nanodiamonds as pH-switchable oxidation and reduction catalysts with enzyme-like activities for immunoassay and antioxidant applications, Nanoscale 9 (2017) 15673–15684.

[19] K. Santacruz-Gomez, A. Sarabia-Sainz, M. Acosta-Elias, M. Sarabia-Sainz, W. Janetanakit, N. Khosla, R. Melendrez, M.P. Montero, R. Lal, Antioxidant activity of hydrated carboxylated nanodiamonds and its influence on water γ-radiolysis, Nanotechnology 29 (2018) 125707, https://doi.org/10.1088/1361-6528/aaa80e.

[20] S. Teerasong, A. Jinnarak, S. Chaneam, P. Wilairat, D. Nacapricha, Poly(vinyl alcohol) capped silver nanoparticles for antioxidant assay based on seed-mediated nanoparticle growth, Talanta 170 (2017) 193–198, https://doi.org/10.1016/j.talanta.2017.04.009.

[21] Y. Zeng, W. Liu, R. Wang, Bio-inspired polydopamine surface modification of nanodiamonds and its reduction of silver nanoparticles, JoVE 141 (2018) e58458–e58465.

[22] Z. Wang, Y. Huang, D. Lv, G. Jiang, F. Zhang, A. Song, Tea polyphenol-assisted green synthesis of Ag-nanodiamond hybrid and its catalytic activity towards 4-nitrophenol reduction, Green Chem. Lett. Rev. 12 (2019) 197–207, https://doi.org/10.1080/17518253.2019.1624836.

[23] Z. Wang, F. Zhang, A. Ning, D. Lv, G. Jiang, A. Song, Nanosilver supported on inert nano-diamond as a direct plasmonic photocatalyst for degradation of methyl blue, J. Environ. Chem. Eng. 9 (2021) 104912, https://doi.org/10.1016/J.JECE.2020.104912.

[24] Y. Zeng, W. Liu, Z. Wang, S. Singamaneni, R. Wang, Multifunctional surface modification of nanodiamonds based on dopamine polymerization, Langmuir 34 (2018) 4036–4042, https://doi.org/10.1021/acs.langmuir.8b00509.

[25] B. Habibi, M. Jahanbakhshi, Sensitive determination of hydrogen peroxide based on a novel nonenzymatic electrochemical sensor: silver nanoparticles decorated on nanodiamonds, J. Iran. Chem. Soc. 12 (2015) 1431–1438.

[26] S.Y. Ong, R.J.J. Van Harmelen, N. Norouzi, F. Offens, I.M. Venema, M.B.H. Najafi, R. Schirhagl, Interaction of nanodiamonds with bacteria, Nanoscale 10 (2018) 17117–17124.

[27] O. Bolshakova, V. Lebedev, E. Mikhailova, O. Zherebyateva, L. Aznabaeva, V. Burdakov, Y. Kulvelis, N. Yevlampieva, A. Mironov, I. Miroshnichenko, Fullerenes on a nanodiamond platform demonstrate antibacterial activity with low cytotoxicity, Pharmaceutics 15 (2023) 1984.

[28] P. Karami, S.A. Aktij, B. Khorshidi, M.D. Firouzjaei, A. Asad, M. Elliott, A. Rahimpour, J.B.P. Soares, M. Sadrzadeh, Nanodiamond-decorated thin film composite membranes with antifouling and antibacterial properties, Desalination 522 (2022) 115436, https://doi.org/10.1016/j.desal.2021.115436.

[29] A. Chatterjee, E. Perevedentseva, M. Jani, C.-Y. Cheng, Y.-S. Ye, P.-H. Chung, C.-L. Cheng, Antibacterial effect of ultrafine nanodiamond against gram-negative bacteria Escherichia coli, J. Biomed. Opt. 20 (2015) 51014.

[30] N. Norouzi, Y. Ong, V.G. Damle, M.B. Habibi Najafi, R. Schirhagl, Effect of medium and aggregation on antibacterial activity of nanodiamonds, Mater. Sci. Eng. C 112 (2020) 110930, https://doi.org/10.1016/j.msec.2020.110930.

[31] W. Cao, X. Peng, X. Chen, X. Wang, J. Feng, Q. Li, H. Chen, C. Jiang, Z. Ye, X. Xing, Facile synthesis of cationic polymer functionalized nanodiamond with high dispersity and antibacterial activity, (n.d.). https://doi.org/10.1007/s10853-016-0475-6..

[32] Y.I. Openda, B.P. Ngoy, T. Nyokong, Photodynamic antimicrobial action of asymmetrical porphyrins functionalized silver-detonation nanodiamonds nanoplatforms for the suppression of staphylococcus aureus planktonic cells and biofilms, Front. Chem. 9 (2021) 628316.

[33] C. Quan, H. Lin, H. Xiao, J. Zhao, Inhibitory effect of carboxylated nanodiamond on oral pathogenic bacteria Streptococcus mutans, J. Clin. Lab. Anal. 35 (2021) e23872.

[34] A. Cumont, A.R. Pitt, P.A. Lambert, M.R. Oggioni, H. Ye, Properties, mechanism and applications of diamond as an antibacterial material, Functional Diamond 1 (2022) 1–28.

[35] S. Szunerits, A. Barras, R. Boukherroub, Antibacterial applications of nanodiamonds, Int. J. Environ. Res. Publ. Health 13 (2016) 413, https://doi.org/10.3390/ijerph13040413.

[36] G. Franci, A. Falanga, S. Galdiero, L. Palomba, M. Rai, G. Morelli, M. Galdiero, Silver nanoparticles as potential antibacterial agents, Molecules 20 (2015) 8856–8874.

[37] B.-M. Chang, L. Pan, H.-H. Lin, H.-C. Chang, Nanodiamond-supported silver nanoparticles as potent and safe antibacterial agents, Sci. Rep. 9 (2019) 13164, https://doi.org/10.1038/s41598-019-49675-z.

[38] T. Xu, L. Wu, Y. Yu, W. Li, J. Zhi, Synthesis and characterization of diamond–silver composite with anti-bacterial property, Mater. Lett. 114 (2014) 92–95, https://doi.org/10.1016/j.matlet.2013.09.119.

[39] S. Iqbal, M.S. Rafique, M. Zahid, S. Bashir, M.A. Ahmad, R. Ahmad, Impact of carrier gas flow rate on the synthesis of nanodiamonds via microplasma technique, Mater. Sci. Semicond. Process. 74 (2018) 31–41.

[40] M. Balouiri, M. Sadiki, S.K. Ibnsouda, Methods for in vitro evaluating antimicrobial activity: a review, J Pharm Anal 6 (2016) 71–79, https://doi.org/10.1016/J.JPHA.2015.11.005.

[41] S.M. Hosseinpour-Mashkani, M. Ramezani, Silver and silver oxide nanoparticles: synthesis and characterization by thermal decomposition, Mater. Lett. 130 (2014) 259–262.

[42] S. Iqbal, M.S. Rafique, S. Akhtar, N. Iqbal, F. Idrees, A. Mahmood, Role of hydrogen flow rate for the growth of quality nanodiamonds via microplasma technique, Materials Innovations 2 (2022) 214–224, https://doi.org/10.54738/MI.2022.2804.

[43] S. Iqbal, M.S. Rafique, S. Akhtar, N. Liaqat, N. Iqbal, R. Ahmad, A comparative study on finding an effective root for the introduction of hydrogen into microplasma during diamond growth, J. Phys. Chem. Solid. 122 (2018) 72–86.

[44] P. Dallas, A.B. Bourlinos, P. Komninou, M. Karakassides, D. Niarchos, Silver nanoparticles and graphitic carbon through thermal decomposition of a silver/acetylenedicarboxylic salt, Nanoscale Res. Lett. 4 (2009) 1358.

[45] D. Mariotti, R.M. Sankaran, Microplasmas for nanomaterials synthesis, J. Phys. D Appl. Phys. 43 (2010) 323001.

[46] A. Roy, S.K. Srivastava, S.L. Shrivastava, A.K. Mandal, Hierarchical assembly of nanodimensional silver–silver oxide physical gels controlling nosocomial infections, ACS Omega 5 (2020) 32617–32631, https://doi.org/10.1021/acsomega.0c04957.

[47] B. Ershov, V. Ershov, Electrochemical mechanism of oxidative dissolution of silver nanoparticles in water: effect of size on electrode potential and solubility, Nanomaterials 13 (2023), https://doi.org/10.3390/nano13131907.

[48] N. Zafar, S. Shamaila, J. Nazir, R. Sharif, M.S. Rafique, J. Ul-Hasan, S. Ammara, H. Khalid, Antibacterial action of chemically synthesized and laser generated silver nanoparticles against human pathogenic bacteria, J. Mater. Sci. Technol. 32 (2016) 721–728.

[49] Y. Yang, J. Shi, G. Kawamura, M. Nogami, Preparation of Au–Ag, Ag–Au core–shell bimetallic nanoparticles for surface-enhanced Raman scattering, Scripta Mater. 58 (2008) 862–865.

[50] M.-L. Wu, L.-B. Lai, Synthesis of Pt/Ag bimetallic nanoparticles in water-in-oil microemulsions, Colloids Surf. A Physicochem. Eng. Asp. 244 (2004) 149–157.

[51] S. Mun, B. Yoon, B.H. Cho, W.B. Ko, Synthesis of silica-silver core-shell nanoparticles and catalytic effect, Asian J. Chem. 24 (2012) 4804.

[52] P. Parvathi, A. Jose, M.S. Kala, Alphonsa V. Joseph, Nandakumar Kalarikkal, S. Thomas, Reduced graphene oxide/silver nanohybrid as a multifunctional material for antibacterial, anticancer, and SERS applications, Appl. Phys. A 126 (2020) 58, https://doi.org/10.1007/s00339-019-3237-x.

[53] O.A. Shenderova, D.M. Gruen, Ultrananocrystalline Diamond: Synthesis, Properties and Applications, second, William Andrew, 2012.

[54] A.B. de Paiva, L.M.B. Vargas, M.J. da Silva, A.D.G. Rodrigues, D.A.W. Soares, M.L. Peres, M.P.F. de Godoy, The negative photoconductivity of Ag/AgO grown by spray-pyrolysis, Surfaces 5 (2022) 209–217, https://doi.org/10.3390/SURFACES5010014.

[55] H. Peng, H. Guo, P. Gao, Y. Zhou, B. Pan, B. Xing, Reduction of silver ions to silver nanoparticles by biomass and biochar: mechanisms and critical factors, Sci. Total Environ. 779 (2021) 146326, https://doi.org/10.1016/j.scitotenv.2021.146326.

[56] S.U. Rehman, S.M. Shah, M. Siddiq, Synthesis and optical studies of silver nanoparticles (Ag NPs) and their hybrids of smart polymer microgel, J. Chem. Soc. Pakistan 35 (2013).

[57] T. Zhao, R. Sun, S. Yu, Z. Zhang, L. Zhou, H. Huang, R. Du, Size-controlled preparation of silver nanoparticles by a modified polyol method, Colloids Surf. A Physicochem. Eng. Asp. 366 (2010) 197–202.

[58] A. Kumar, P.A. Lin, A. Xue, B. Hao, Y.K. Yap, R.M. Sankaran, Formation of nanodiamonds at near-ambient conditions via microplasma dissociation of ethanol vapour, Nat. Commun. 4 (2013).

[59] S. Prasetyo, Zaitun Isnaeni, K. Mitchell, M.M. Suliyanti, Y. Herbani, Analyzing silver concentration in soil using laser-induced breakdown spectroscopy, J Phys Conf Ser 985 (2018) 012009, https://doi.org/10.1088/1742-6596/985/1/012009.

[60] J.M. Vadillo, S. Palanco, M.D. Romero, J.J. Laserna, Applications of laser-induced breakdown spectrometry (LIBS) in surface analysis, Fresenius' J. Anal. Chem. 355 (1996) 909–912, https://doi.org/10.1007/s0021663550909.

[61] M.A. El-Naka, A. El-Dissouky, G.Y. Ali, S. Ebrahim, A. Shokry, Garlic capped silver nanoparticles for rapid detection of cholesterol, Talanta 253 (2023) 123908, https://doi.org/10.1016/j.talanta.2022.123908.

[62] G. Eastmond, H. Höcker, D. Klee, Biomedical Applications Polymer Blends, Springer, 2003.

[63] A. Shah, S. Haq, W. Rehman, M. Waseem, S. Shoukat, M. Rehman, Photocatalytic and antibacterial activities of paeonia emodi mediated silver oxide nanoparticles, Mater. Res. Express 6 (2019) 045045, https://doi.org/10.1088/2053-1591/aafd42.

[64] M. Chennimalai, T.S. Senthil, M. Kang, N. Senthilkumar, A novel green-mediated approach of 3-D hierarchical-like ZnO@Ag, ZnO@Au and ZnO@Ag@Au NCs prepared via Opuntia ficus indica fruits extract for enhancement of biological activities, Appl. Phys. A 127 (2021) 611, https://doi.org/10.1007/s00339-021-04768-3.

[65] E.E. Elemike, D.C. Onwudiwe, A.C. Ekennia, C.U. Sonde, R.C. Ehiri, Green synthesis of Ag/Ag2O nanoparticles using aqueous leaf extract of eupatorium odoratum and its antimicrobial and mosquito larvicidal activities, Molecules 22 (2017), https://doi.org/10.3390/molecules22050674.

[66] M. Abbasi, R. Gholizadeh, S.R. Kasaee, A. Vaez, S. Chelliapan, F. Fadhil Al-Qaim, I.F. Deyab, M. Shafiee, Z. Zareshahrabadi, A.M. Amani, An intriguing approach toward antibacterial activity of green synthesized Rutin-templated mesoporous silica nanoparticles decorated with nanosilver, Sci. Rep. 13 (2023) 5987.

[67] N. Iqbal, M.R.A. Kadir, N.H. Bin Mahmood, S. Iqbal, D. Almasi, F. Naghizadeh, H.R. Balaji, T. Kamarul, Characterization and biological evaluation of silver containing fluoroapatite nanoparticles prepared through microwave synthesis, Ceram. Int. 41 (2015) 6470–6477.

[68] Y. Sadeghipour, M.H. Alipour, H.R. Ghaderi Jafarbeigloo, A. Salahvarzi, M. Mirzaii, A.M. Amani, S. Mosleh-shirazi, M. Mehrabi, Evaluation antibacterial activity of biosynthesized silver nanoparticles by using extract of Euphorbia Pseudocactus Berger (Euphorbiaceae), Nanomedicine Research Journal 5 (2020) 265–275.

[69] W.K.A. Wan Mat Khalir, K. Shameli, S.D. Jazayeri, N.A. Othman, N.W. Che Jusoh, N.M. Hassan, Biosynthesized silver nanoparticles by aqueous stem extract of Entada spiralis and screening of their biomedical activity, Front. Chem. 8 (2020) 620.

[70] A. Lange, E. Sawosz, M. Wierzbicki, M. Kutwin, K. Daniluk, B. Strojny, A. Ostrowska, B. Wójcik, M. Łojkowski, M. Gołębiewski, Nanocomposites of graphene oxide—silver nanoparticles for enhanced antibacterial activity: mechanism of action and medical textiles coating, Materials 15 (2022) 3122.

[71] Y.-X. Pan, Q.-H. Xu, H.-M. Xiao, C.-Y. Li, Insights into the antibacterial activity and antibacterial mechanism of silver modified fullerene towards Staphylococcus aureus by multiple spectrometric examinations, Chemosphere 342 (2023) 140136, https://doi.org/10.1016/j.chemosphere.2023.140136.

[72] S. V Gudkov, D.A. Serov, M.E. Astashev, A.A. Semenova, A.B. Lisitsyn, Ag2O nanoparticles as a candidate for antimicrobial compounds of the new generation, Pharmaceuticals 15 (2022) 968.
[73] L. Wang, C. Hu, L. Shao, The antimicrobial activity of nanoparticles: present situation and prospects for the future, Int. J. Nanomed. (2017), https://doi.org/10.2147/IJN.S121956, 12–1227.
[74] A. Lange, E. Sawosz, M. Wierzbicki, M. Kutwin, K. Daniluk, B. Strojny, A. Ostrowska, B. Wójcik, M. Łojkowski, M. Gołębiewski, A. Chwalibog, S. Jaworski, Nanocomposites of graphene oxide—silver nanoparticles for enhanced antibacterial activity: mechanism of action and medical textiles coating, Materials 15 (2022), https://doi.org/10.3390/ma15093122.
[75] A.S. Pozdnyakov, A.I. Emel'yanov, N.P. Kuznetsova, T.G. Ermakova, S.A. Korzhova, S.S. Khutsishvili, T.I. Vakul'skaya, G.F. Prozorova, Synthesis and characterization of silver-containing nanocomposites based on 1-Vinyl-1,2,4-triazole and acrylonitrile copolymer, J. Nanomater. 2019 (2019) 4895192, https://doi.org/10.1155/2019/4895192.
[76] Y. Wu, Y. Yang, Z. Zhang, Z. Wang, Y. Zhao, L. Sun, Fabrication of cotton fabrics with durable antibacterial activities finishing by Ag nanoparticles, Textil. Res. J. 89 (2019) 867–880.